Assembly Dynamics of the Nucleocapsid Shell Subunit (P8) of Bacteriophage ϕ6†

Roman Tuma,‡,§ Jaana K. H. Bamford,|| Dennis H. Bamford,|| and George J. Thomas, Jr.*,‡

Division of Cell Biology & Biophysics, School of Biological Sciences, University of Missouri-Kansas City, Kansas City, Missouri 64110, and Department of Biosciences and Institute of Biotechnology, Viikki Biocenter, University of Helsinki, Helsinki, Finland

Received June 28, 1999; Revised Manuscript Received September 16, 1999

ABSTRACT: ϕ6 is an enveloped dsRNA bacteriophage of *Pseudomonas syringae*. The viral envelope encloses a nucleocapsid, consisting of an RNA-dependent RNA polymerase complex within an icosahedral shell assembled from approximately 800 copies of a 16 kDa subunit (protein P8, encoded by viral gene 8). During infection, the nucleocapsid penetrates the host plasma membrane and enters the cytosol, whereupon the P8 shell disassembles and the polymerase complex is activated. To understand the molecular mechanisms of shell assembly and disassembly—processes that have counterparts in most viral infections—we have investigated the structure, stability, and dynamics of P8 in different assembly states using time-resolved Raman spectroscopy and hydrogen-isotope exchange. In the presence of Ca^{2+}, which promotes shell assembly, the highly α-helical conformation of the P8 subunit is stabilized by rapid assembly into shell-like structures. However, in the absence of Ca^{2+}, the P8 subunit is thermolabile and unstable, manifested by a slow α-helix → β-strand conformational change and the accumulation of aberrant aggregates. In both properly assembled shells and aberrant aggregates, the P8 subunit retains an α-helical core that is protected against deuterium exchange of amide NH groups. Surprisingly, no additional protection against amide exchange is conferred by the shell lattice. Time-resolved assembly and disassembly experiments in deuterated buffers indicate that the regions of P8 involved in subunit/subunit interactions in the intact shell undergo rapid exchanges, presumably due to local unfolding events that are characterized by low activation barriers. Such localized dynamics of P8 within the shell lattice may mediate the nucleocapsid/host membrane interactions that are required in the cytosol for particle assembly during maturation and disassembly during infection.

Many cellular functions, including replication, transcription, translation, energy transduction, and membrane translocation, depend on complex recognition events and conformational changes of macromolecules. Viruses can serve as useful models for studying the molecular mechanisms underlying such cellular functions. For example, the life cycle of a virus typically requires the assembly of a capsid from protein subunits, the packaging within of a genome, and the execution of receptor-mediated cell entry. Thus, the capsid protein must undergo a variety of structural transformations on the basis of information encoded within its sequence. Studies of capsid association and dissociation properties therefore have the potential to provide insights into structural principles governing similar phenomena of more complex cellular assemblies. A particularly appropriate viral model is the nucleocapsid of the dsRNA bacteriophage ϕ6, which functions as an RNA-dependent RNA polymerase machine.

ϕ6, an enveloped double-stranded (ds)[1] RNA virus that infects the phytopathogenic bacterium *Pseudomonas syringae*, is structurally and functionally similar to viruses of the *reoviridae* family (*1, 2*). The viral envelope encloses a nucleocapsid (NC) consisting of an inner core of three genomic dsRNA segments in combination with four protein species (P1, P2, P4, and P7) plus an outer shell constructed from multiple copies of a 16 kDa protein (P8, encoded by viral gene 8). The P8 shell is assembled in vivo around the NC at the cytoplasmic side of the plasma membrane. Recognition between the membrane and the NC is presumably mediated by the P8 shell.

The RNA-dependent RNA polymerase activity of ϕ6 is associated with protein P2 of the inner core particle. The NC enters the host cell by penetrating the plasma membrane in an endocytotic event that is dependent upon membrane potential (*3*). After cell entry, the shell disassembles, releasing its core and activating the polymerase. Conversely, polymerase activity is inhibited by assembly of the P8 shell around the core (*4*−*6*). The first intermediate detected postinfection is a proteinaceous particle, referred to as the

† This work was supported by Grants GM50776 from the U.S. National Institutes of Health (to G.J.T.), B104-CT97-2364 from the European Union (to D.H.B.), and 37725 and 62993 from the Finnish Academy of Sciences (to D.H.B.). This paper is part LXX in the series Studies of Virus Structure by Raman Spectroscopy.

* To whom correspondence should be addressed.

‡ University of Missouri-Kansas City.

§ Present address: Department of Biosciences, Biocenter, University of Helsinki, Finland.

|| University of Helsinki.

[1] Abbreviations: BTV, blue tongue virus; ds, double-stranded; EGTA, ethylene glycol-bis-(β-aminoethyl ether)-*N*,*N*,*N*′,*N*′-tetraacetic acid; kDa, kilodalton; NC, nucleocapsid of ϕ6; PC, procapsid of ϕ6; SDS−PAGE, sodium docecyl sulfate−polyacrylamide gel electrophoresis.

10.1021/bi991473p CCC: $18.00
Published on Web 10/16/1999

Table 1: Raman Band Frequencies and Assignments for the P8 Subunit in H_2O and D_2O Solutions

cm^{-1} (H_2O)[a]	cm^{-1} (D_2O)[a]	assignment[b]
622	622	Phe
643	642	Tyr
825	827	Tyr
853	851	Tyr
904		Ala
	910	amide III′ (turns/coil); various side chains
	927	amide III′ (turns/β-strand)
936		C−C stretching
	953	amide III′ (α-helix)[c]
	963	amide III′ (coil)[d]
	984	amide III′ (turns/β-strand)
1004	1003	Phe
1032	1032	Phe
1063		Lys, Arg; C−N stretching
1104		peptide C−N stretching[d]
1126		peptide C−N stretching[d]
1174	1174	Tyr
1208	1208	Tyr
1238		amide III (turns/β-strand)
1264	1260	Tyr
1275		amide III (α-helix)
1300		amide III (α-helix)
1318	1318	various side chains; C−H deformation
1342	1342	various side chains; C−H deformation
1342	1298	α-helix mainchain; (O═C)-C^{α}-H group[e]
1416	1404	Asp, Glu; CO_2- stretching
	1400−1500	amide II′ (α-helix)
1451	1451	various side chains, CH_2 deformation
1617	1614	Tyr
1645−1654	1633−1640	amide I/I′ (α-helix)
1665−1672	1655	amide I/I′ (nonhelical)

[a] Frequencies are accurate to ± 1 cm^{-1}. [b] Assignments are from refs *13*, *17*, *26*, *30*, *34*, and *38*, except as indicated otherwise. [c] From refs *39*, *50*, and *51*. [d] From ref *39* and unpublished results of R. Tuma and G. J. Thomas, Jr. [e] From ref *33*.

procapsid (PC) (*7*, *8*). The PC contains the same four proteins as the core particle, viz., P1, P2, P4, and P7, but is free of RNA. As in the case of the core particle, a shell of P8 subunits can assemble around the PC. Image reconstructions based upon electron cryomicroscopy reveal that the P8 shell of the PC conforms to $T = 13$ icosahedral symmetry (*9*). The sequence of P8 is rich in acidic residues and has a high propensity for α-helix, as confirmed experimentally by Raman analysis (*10*). Assembly of the P8 shell around the core can be triggered in vitro by addition of 0.1−1.0 mM Ca^{2+}, and the resulting NC particles are infectious to host cell spheroplasts (*11*). Conversely, disassembly of the NC shell is driven by millimolar quantities of the Ca^{2+} chelator, EGTA. Interestingly, the generation of a shell-like state from purified P8 can be achieved even in the absence of the core. Although such particles exhibit the expected size, shape, and local symmetry of the native shell lattice, most are not closed shells. Nevertheless, these shell-like assemblies can be used to model intersubunit contacts of the native P8 shell. Similarly, the purified P8 subunit can be used as a model for both the shell precursor state and the disassembled shell subunit.

Raman spectroscopy has been demonstrated as an effective probe of subunit structure and dynamics in viruses and viral precursor particles (*12*−*16*). Raman spectra are particularly sensitive to small changes in subunit secondary and tertiary structures that accompany transformations in capsid morphology along the assembly pathway (*16*−*18*). Raman methods have been applied successfully to ϕ6 assembly intermediates, including the mature virion and membrane-associated structural proteins of the virus (*10*, *12*). Most recently, the RNA-packaging NTPase of ϕ6 (protein P4) has been probed by Raman difference methods to identify conformational changes attendant with nucleoside triphosphate binding and hydrolysis (*19*).

The relatively low solubility of the P8 protein in the absence of Ca^{2+} has been a major obstacle in previous efforts to probe details of shell assembly and disassembly by Raman spectroscopy. On the other hand, it has been shown that a time-resolved approach in conjunction with hydrogen-isotope (H → D) exchange can extend the capabilities of Raman spectroscopy to otherwise refractory samples (*16*, *19*). In the present study, we apply the time-resolved Raman and H → D exchange methods to investigate self-assembly of the P8 subunit in vitro. The methods are applied to resolve the sequence of conformational changes taking place during P8 assembly and disassembly processes. The results suggest a model for penetration of the ϕ6 NC particle through the host cytoplasmic membrane.

MATERIALS AND METHODS

Protein Purification. The P8 protein was obtained by sequential disassembly of purified ϕ6 as described previously (*20*). In short, the viral membrane was removed by treatment of ϕ6 with Triton X-114, and the resulting NC particles were treated with EGTA to release P8, which was applied to a Mono Q (Pharmacia) ion-exchange column in 10 mM Tris-HCl, pH 8, and 0.1 mM EGTA buffer. The bound protein was eluted by a NaCl gradient, with P8 eluting at about 300 mM NaCl. A yield of 4 mg of P8 was obtained from 100 mg of purified virus. P8 shells were assembled from purified P8 by addition of Ca^{2+} ($CaCl_2$). The P8 shells were separated from unassembled protein by rate zonal sucrose gradient centrifugation as described (*6*). Protein concentrations were measured by the Bradford assay (*21*) using BSA as a standard. The purity of the protein was assessed by SDS−PAGE (*22*).

Circular Dichroism. Circular dichroism (CD) spectra were recorded from solutions of the P8 subunit (31 μM protein in 10 mM Tris and 150 mM NaCl, pH 7.4, at 20 °C) on a Jasco J-120 instrument, which was calibrated with *d*-camphor sulfonic acid. Multiple scans were averaged and normalized (*23*).

Raman Spectroscopy. Several fresh preparations of P8 subunits were concentrated for Raman spectroscopy using a Centricon-10 microconcentrator (Amicon). The final protein concentration was 50 mg/mL in 10 mM Tris-HCl buffer, 150 mM NaCl, pH 7.4, and 0.1 mM EGTA. P8 shells were assembled from P8 subunit preparations by addition of 1 mM $CaCl_2$ and were separated from unpolymerized protein and aggregates by rate zonal centrifugation.

Temperature-resolved spectra were collected on a Spex 1877 triple spectrograph equipped with a charge-coupled-device detector (*17*). Multiple spectra were collected and averaged at each temperature.

Hydrogen exchange was monitored using a dialysis flow cell device and time-resolved Raman spectroscopy as described previously (*15*, *24*). About 5 μL of P8 solution (50 mg/mL) was loaded into the flow cell and exchanged at

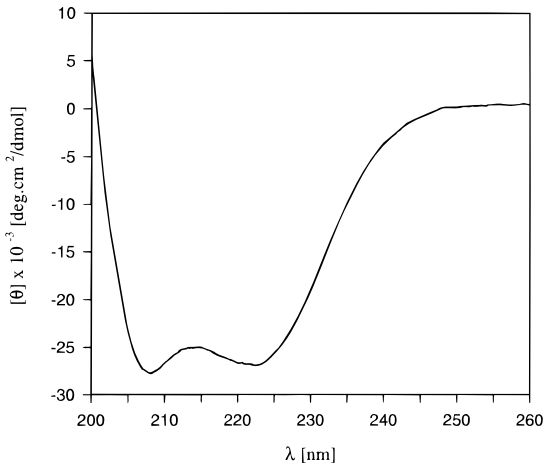

FIGURE 1: Circular dichroism spectrum of P8 protein at 31 μM in 10 mM Tris and 0.15 M NaCl, pH 7.4, buffer at 20 °C.

10 °C against 10 mM Tris-DCl, 150 mM NaCl, and 1 mM $CaCl_2$ (D_2O), pH* = 7.4 (pH* represents the pH value in D_2O solution, without correction for deuterium effects). Spectra were recorded in real time at 1 min intervals. Disassembly of P8 shells was achieved by microdialysis against 5 mM EGTA solution in 10 mM Tris and 150 mM NaCl. Using the microdialysis flow cell device, the half-time for EGTA exchange is ~8 min. Thus, the 2 mM EGTA concentration that is necessary for disassembly is achieved in about 6 min. The kinetics of assembly (in the presence of 1 mM $CaCl_2$) and disassembly (2 mM EGTA) were determined by light scattering, which was monitored by turbidity at 450 nm (*25*).

Temperature-resolved spectra were normalized using the 1003 cm^{-1} band of phenylalanine as an internal intensity standard. The same internal standard was also used for computation of all difference spectra. Reliability of this intensity standard has been demonstrated previously (*12*, *15*).

Time-resolved spectra for hydrogen-exchange experiments were also normalized using the 1003 cm^{-1} band of phenylalanine. The rate of D_2O efflux into the sample was measured using the intensity of the 1206 cm^{-1} band (DOD bending vibration) (*24*). A time-dependent amide III′ envelope was extracted from each set of data using difference spectroscopy and linear least-squares band decomposition as described previously (*15*). Second-order kinetic analysis of the hydrogen-exchange measurements was performed by use of the time-dependent intensity of the 950 cm^{-1} band, an established Raman marker (amide III′ mode) of peptide NH → ND exchange (*24*, *26*).

RESULTS

P8 Subunit Fold Is α-Helical. Figure 1 shows the CD spectrum of the P8 subunit. The well-defined CD minima at 208 and 222 nm are characteristic of a highly α-helical protein. Linear least-squares analysis (*23*) of the data is consistent with the following distribution of secondary structure: 56 ± 10% α-helix, 34 ± 6% coil, 10 ± 4% β-turns, and less than 5% β strand.

Raman spectra of ~3 mM solutions of P8 at various experimental conditions are shown in Figure 2. In the physiological temperature range (10−30 °C) and in the absence of added Ca^{2+}, the P8 Raman spectrum exhibits a sharp amide I band at 1655 cm^{-1} and amide III bands at 1275 and ca. 1300−1318 cm^{-1} (Figure 2, left panel, bottom traces). The observed amide bands are diagnostic of α-helix (*27*−*30*). Additional Raman bands considered characteristic of the α-helical conformation are evident at 932 and 1342 cm^{-1}. The former is associated with side-chain $C^{\alpha}-C^{\beta}$ stretching in helical regions (*31*, *32*) and the latter with coupled $C^{\alpha}-H$ bending plus $C-C^{\alpha}$ stretching motions of the protein mainchain (*33*, *34*). The sharpness of amide I as well as the paucity of Raman amide III intensity in the interval 1230−1240 cm^{-1} is consistent with the absence of appreciable β-strand structure in the P8 subunit (*27*). Decompositions of the Raman amide I band shape (10 °C spectrum) using both reference intensity profiles (*35*) and Fourier deconvolution (*36*) methods provide a consistent estimate of secondary structure (50 ± 4% α-helix, 38 ± 5% coil, and 12 ± 3% turns and β strand), in accord with the CD analysis. Thus, we conclude that the P8 subunit attains a predominantly α-helical fold over a wide concentration range. A similar analysis of the Raman spectrum of P8 in the presence of Ca^{2+} (Figure 2, right panel) suggests the following secondary structure distribution for the P8 subunit of the shell assembly: 57 ± 3% α-helix and 40 ± 5% coil.

Calcium Binding and Subunit Assembly Stabilize P8. Although shell assembly and disassembly do not lead to dramatic changes in the P8 Raman signature (cf. left and right panels of Figure 2), the computed difference spectrum (Figure 3) demonstrates several significant Raman perturbations indicative of a subunit structural transformation. Salient features of the difference spectrum of Figure 3 include troughs at 1238 cm^{-1} (amide III) and 1672 cm^{-1} (amide I) and a peak at 936 cm^{-1} ($C^{\alpha}-C^{\beta}$ stretch), which indicate, respectively, more β-strand and less α-helix in disassembled subunits than in the assembled shell (*31*, *32*). This is in accord with the above curve-fitting analysis, which shows that the assembled shell contains the more highly α-helical secondary structure.

The Figure 3 difference spectrum also provides evidence of a small redistribution of Raman intensity between the pair of tyrosine bands (Fermi doublet) at 832 and 852 cm^{-1}. The spectral change is interpreted as evidence that the average tyrosine phenoxyl group is a somewhat stronger hydrogen-bond acceptor in the shell than in the disassembled subunit (*37*). The small magnitude of the effect is consistent with only one of the six tyrosines per subunit being transformed from a donor to an acceptor role. Additional spectral differences in the 1400−1500 cm^{-1} region are indicative of assembly related changes in the environments of aliphatic side chains (*38*). Finally, the difference trough at 1416 cm^{-1} reflects a likely change in the average environment of carboxyl groups of Asp and Glu upon addition of Ca^{2+} (*31*, *39*).

The qualitative pattern of features in the difference spectrum of Figure 3 was conserved for all fresh preparations of the assembled shells. However, in the case of unassembled subunits, the inherent thermolability of P8, particularly above 30 °C (see below), led to small variations in the magnitudes of difference bands from one preparation to another (data not shown). These variations suggested that spectral differences between the shell and subunit may be due to a relatively slow conformational drift and/or aggregation of the subunit in the disassembled state, inasmuch as similar

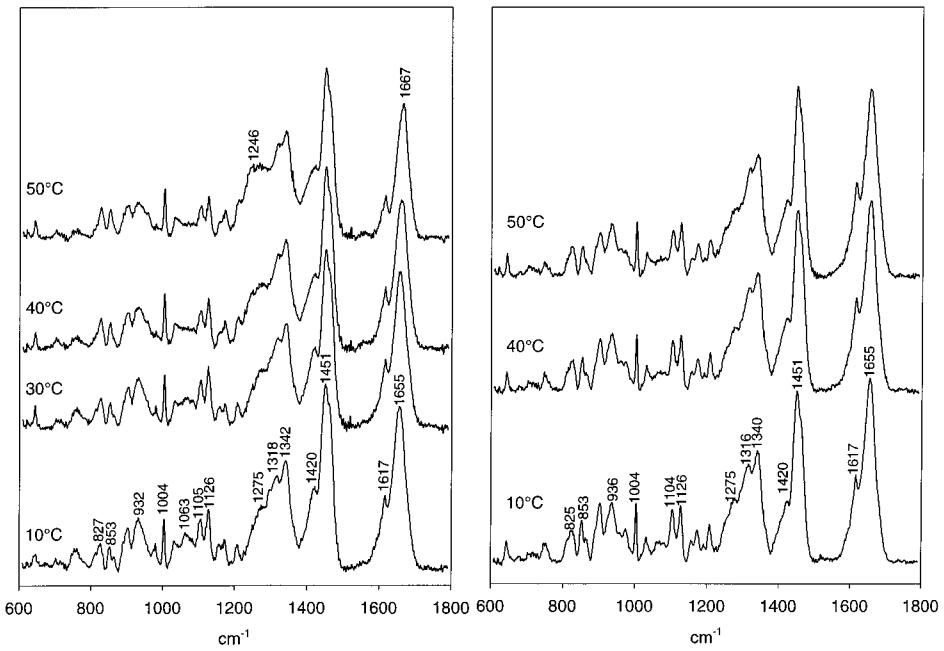

FIGURE 2: Thermostability of P8 assessed by Raman spectroscopy. (Left) Raman spectra of the P8 subunit at 50 mg/mL in 10 mM Tris, 0.15 M NaCl, and 1 mM EGTA, pH 7.4, buffer over the range 10−50 °C. (Right) Raman spectra of the P8 shell at 50 mg/mL in 10 mM Tris, 0.15 M NaCl, and 1 mM $CaCl_2$, pH 7.4, buffer over the range 10−50 °C. Spectra are corrected for buffer contributions and normalized as described in the text.

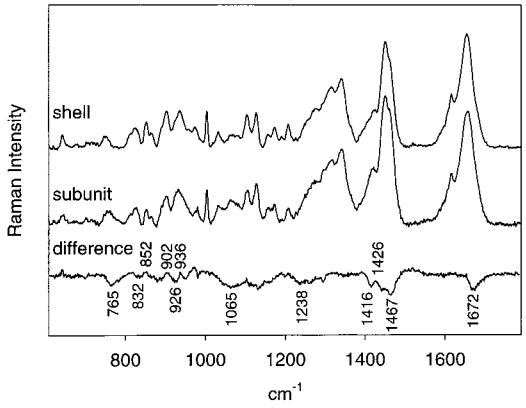

FIGURE 3: Comparison of Raman spectra of the P8 shell and subunit at 10 °C. Spectra (from Figure 2) are corrected for buffer contributions and normalized as described in the text.

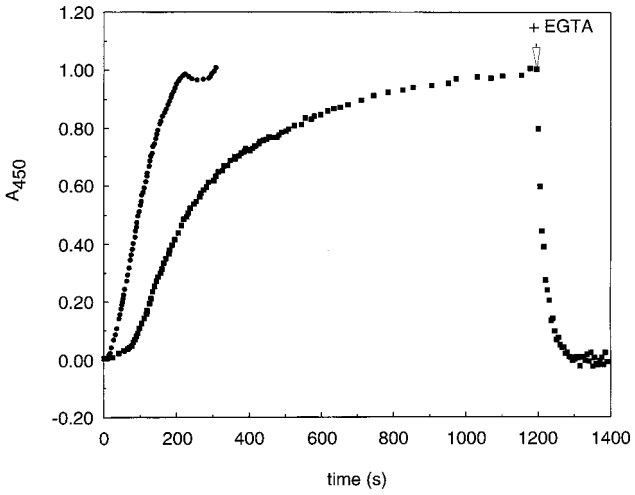

FIGURE 4: P8 assembly and disassembly monitored by turbidity at 450 nm, using P8 concentrations of 0.25 (squares) and 1 (circles) mg/mL in 10 mM Tris and 0.15 M NaCl, pH 7.4, buffer. Disassembly of p8 at 0.25 mg/mL was triggered by rapid addition of an aliquot of EGTA (0.2 M) to obtain a final concentration of 2 mM, as indicated by the arrow. The assembly at 1 mg/mL was not fully reversible and resulted in visible aggregation, represented by the ripples in the plateau region of the curve.

variations were not observed for different preparations of the assembled shells. The spectral differences between shells and subunits were further investigated by time-resolved Raman spectroscopy, as described below.

Despite the relatively small scale of spectral and structural changes in the P8 subunit accompanying assembly/disassembly, the thermostabilities of the two states differ appreciably. Thus, between 30 and 50 °C, amide I of the subunit is shifted from 1655 to 1667 cm^{-1} (Figure 2, left panel), whereas amide I of the shell is virtually unshifted (Figure 2, right panel). Likewise, significant temperature-induced changes in amide III and in the 932 cm^{-1} marker occur for the subunit (Figure 2), but not for the shell (Figure 3). All of the data are consistent with a temperature-induced α-helix → β-strand transformation between 30 and 50 °C for the disassembled subunit, but not for the assembled shell. Further, at the protein concentrations employed in these experiments (i.e., ∼50 mg/mL or ∼3 mM in subunits) the disassembled subunits aggregate irreversibly above 50 °C, whereas the assembled shells remain intact during prolonged incubation at 50 °C. Thus, shell assembly confers substantial thermostabilization to the P8 subunit.

Mechanisms of P8 Assembly and Disassembly Investigated by Time-Resolved Raman Spectroscopy. Assembly and disassembly of the P8 shell are controlled by Ca^{2+} (*6*). To establish the kinetics of shell assembly and disassembly, we used a simple turbidity assay (Figure 4). At 1 mg/mL, P8 assembly is rapid and largely irreversible, resulting in visible precipitation. On the other hand, at 0.25 mg/mL, the assembly/disassembly reaction is fully reversible. At the lower concentration, a significant lag phase is discernible, which is likely due to nucleation-limited polymerization (*25*).

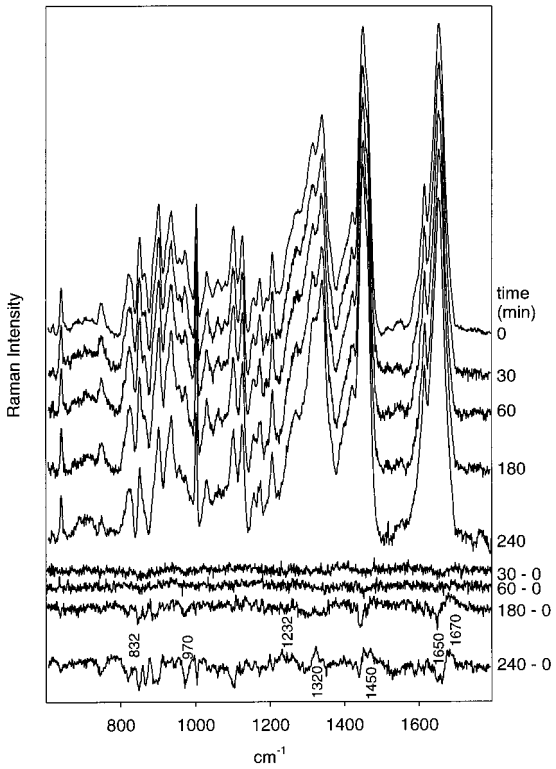

FIGURE 5: Time-resolved Raman spectra of P8 shells disassembled in a Raman microdialysis flow cell (*24*). P8 shells (70 mg/mL) in 10 mM Tris, 0.15 M NaCl, and 1 mM $CaCl_2$, pH 7.4, buffer were dialyzed against 10 mM Tris, 0.15 M NaCl and 2 mM EGTA, pH 7.4, buffer. The buffer exchange was completed in less than 15 min (*24*). Raman spectra were collected at 1 min intervals. The times indicated for different slots and their corresponding difference spectra (bottom of figure) were measured from the start of the dialysis procedure. Difference spectra were obtained using methods described in the text.

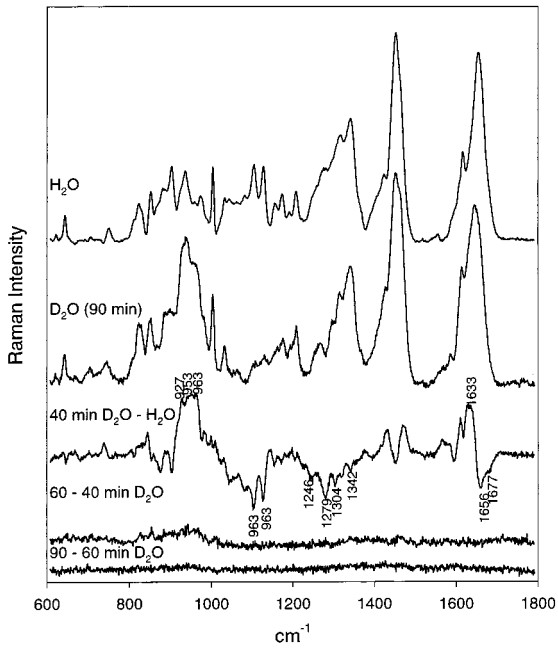

FIGURE 6: Hydrogen−deuterium exchange of the P8 shell as monitored by Raman spectroscopy. The D_2O spectrum was obtained after 90 min in D_2O Tris buffer (pH* 7.4) containing Ca^{2+} at 10 °C. Sequential differences between spectra of P8 shells exchanged for different times are shown in the lower traces.

EGTA-triggered depolymerization is complete in less than 2 min, characterized by an apparent first-order rate constant of ~2.8 min^{-1}.

To investigate shell depolymerization (disassembly), we employed a Raman microdialysis device that permits collection of Raman spectra in real time while the Ca^{2+}-containing buffer is exchanged by 2 mM EGTA-containing buffer. This buffer exchange is governed by a rate of ~0.07 min^{-1} (*24*), which is sufficient to decrease [Ca^{2+}] below the threshold for assembly (0.5 mM) within 10 min. Below this threshold, the P8 shells disintegrate into subunits in less than 1 min (Figure 4). Thus, any subunit structural transformations concomitant with shell disassembly should be detectable within the 10 min window.

Time-resolved Raman spectra as a function of EGTA dialysis are shown in Figure 5. The data demonstrate that even after depleting Ca^{2+} for 30 min no significant spectral change occurs. Incubation of the subunits in EGTA at 10 °C for an additional 30 min also produces no discernible effect. The first significant change in P8 secondary structure appears 3 h after Ca^{2+} depletion and becomes more pronounced after 4 h, as revealed by the trough at 1650 cm^{-1} and peaks near 1670 and 1232 cm^{-1} in the difference spectra of Figure 5. The amide difference bands signify a conversion from α-helix to β-strand. The additional features at 830/850 (doublet), 970, and 1440 cm^{-1} indicate accompanying changes in the environments of tyrosine and aliphatic side chains. Many of the difference features attendant with shell depolymerization (Figure 5, bottom trace) resemble those observed in the difference spectrum between shell and subunits (Figure 3, bottom trace), indicating that P8 subunits undergo similar structural transitions in the two cases.

It is important to note, however, that the spectral changes revealed in Figure 5 are not due to disassembly per se. Rather, they reflect *both* the local destabilization of the subunit structure following disruption of subunit−subunit contacts of the assembled shell *and* the stabilization of an alternative β-strand secondary structure. The onset of these spectral changes lags behind disassembly and resembles a nucleation-limited polymerization. Therefore, the structural changes are likely due to off-pathway aggregation. The spectral signature suggests that the destabilized native secondary structure is α-helical and that altered tertiary structural contacts of tyrosine and aliphatic residues also take place.

Hydrogen-Isotope Exchange. Bacteriophage ϕ6 morphogenesis requires that P8 subunits assemble into a shell around the NC core during maturation and subsequently disassemble upon entry of the NC into the host cell. Such metastability of the NC shell must be engineered into the P8 subunit, presumably through inherent conformational flexibility, not unlike that observed in the procapsid shells of dsDNA viruses (*16*). A sensitive measure of conformational flexibility of the P8 subunit within the shell assembly can be obtained from the extent and kinetics of hydrogen-isotope exchange (*16*, *24*, *26*). We have examined the P8 shell for this purpose using the Raman microdialysis device described above.

Figures 6 and 7 show that at 10 °C a large population of amide (NH) protons in subunits of the P8 shell exchanges rapidly, i.e., within 40 min of exposure to D_2O. This population includes about 50% of the α-helical NH sites and the vast majority of NH groups in nonhelical conformations.

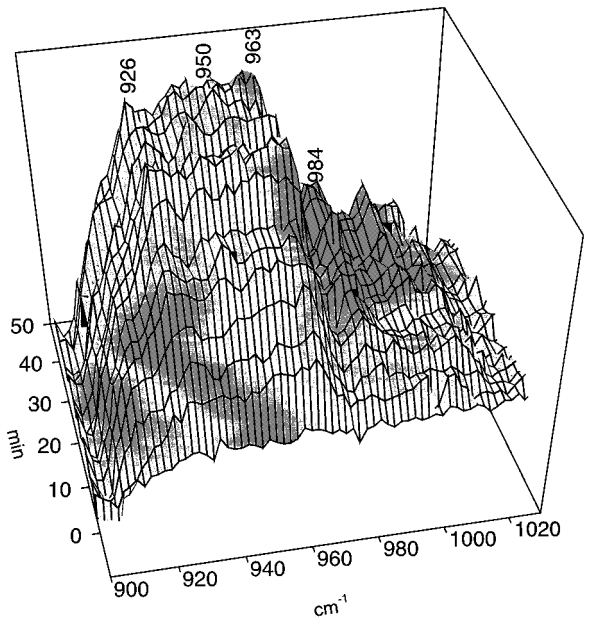

FIGURE 7: Time-resolved fast phase of exchange (0−30 min) monitored by bands of the amide III′ region. The amide III′ bands were extracted by subtraction of the P8 spectrum recorded in H_2O.

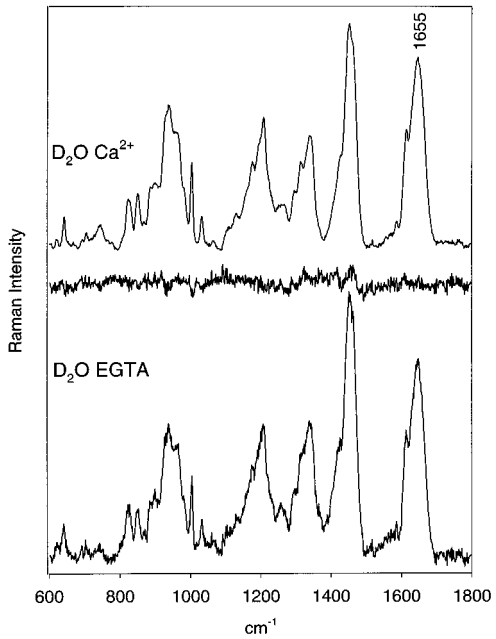

FIGURE 8: Hydrogen−deuterium exchange during P8 shell disassembly in D_2O, as monitored by time-resolved Raman spectroscopy. The top trace represents the spectrum of the P8 shell after 90 min in D_2O. The bottom trace represents the spectrum of the same P8 shells after disassembly in D_2O. The middle trace is the difference between the top and bottom traces. Other conditions are as given in the legend of Figure 6.

Virtually no additional amide exchange takes place in the subsequent 50 min. The amide III′ profile resulting from NH → ND exchange consists of a broad band centered near 950−953 cm^{-1}, which is diagnostic of the exchange of α-helices in the native state. As expected, difference troughs also occur in the amide I (1656 cm^{-1}) and amide III (1279 cm^{-1}) regions corresponding to exchange of these α-helices. The additional amide III′ satellites at 930 and 963 cm^{-1} likely represent regions of exchanged coil (disordered) and turn secondary structures.

Although the α-helix population exchanging from the native state at 10 °C is substantial (∼50%), additional exchange of α-helices is detected at higher temperature (50 °C, data not shown). The latter presumably represent subunit domains in the shell assembly that become unfolded at 50 °C. This additional exchange at the higher temperature shows that P8 does not exchange completely in the native (10 °C) assembled state.

To further characterize the exchange-protected NH groups, the natively exchanged shells (10 °C) were disassembled into subunits in 2 mM EGTA-D_2O buffer at 10 °C, and the Raman spectrum was again recorded. The Raman signature (Figure 8) reveals no additional NH exchange up to 90 min after disassembly at 10 °C, indicating that assembled and disassembled states of P8 have approximately the same relative populations of exchangeable (unprotected) and nonexchangeable (protected) NH groups at native conditions. Within the time resolution of the method (∼1 min), the exchange kinetics of shells and disassembled subunits are also rather similar. [A very small exchange retardation observed for P8 shells vis-à-vis disassembled P8 subunits corresponds to a local stabilization of no more than ∼1−2 kcal/mol (*15*).] Thus, solvent-accessible helices of the P8 subunit remain largely accessible in the shell assembly. These results are consistent with a model for the P8 shell in which local unfolding and NH exchange of helices are not greatly hindered by quaternary contacts. On the other hand, the folding core of the P8 subunit is apparently stabilized by the shell lattice, as manifested by the greater thermostability of the shell. The increased global stability of the shell subunit is presumably due to the binding of Ca^{2+}, which is also expected to affect processes coupled to it (e.g., global but not local unfolding).

As noted above, approximately 50% of the α-helical NH sites of the native subunit are unprotected at 10 °C, and the remaining 50% become largely unprotected at 50 °C. At the latter temperature both the shell assembly and native subunit conformation are destabilized. Therefore, helix exchange at 50 °C may occur via both local and global unfolding mechanisms. This is consistent with the expectation (based upon Raman and CD signatures) that the folding core of the P8 subunit is substantially α-helical.

DISCUSSION

P8 Is an α-Helical Capsid Subunit. The spectroscopic results reported here and previously (*10*) demonstrate that the nucleocapsid shell subunit, P8, of bacteriophage ϕ6 is a highly α-helical protein. As such, it is a member of the growing family of structural proteins of icosahedral viruses exhibiting the α-helical fold. Included in this group are the core antigen of the hepatitis B virus (*40*), several retrovirus capsid proteins (*41*−*43*), and the α-helical domain of the blue tongue virus (BTV) core protein VP7 (*44*, *45*). The last is a functional counterpart of P8, and interestingly, its α-helical domain exhibits similar size (16 kDa) though no apparent sequence homology with P8. Additionally, both ϕ6 and BTV share a similar viral architecture, including an encapsidated polymerase core. The rotavirus homolog, VP6, aids in transient envelopment of the viral particle utilizing direct membrane interactions in a fashion similar to P8 of ϕ6.

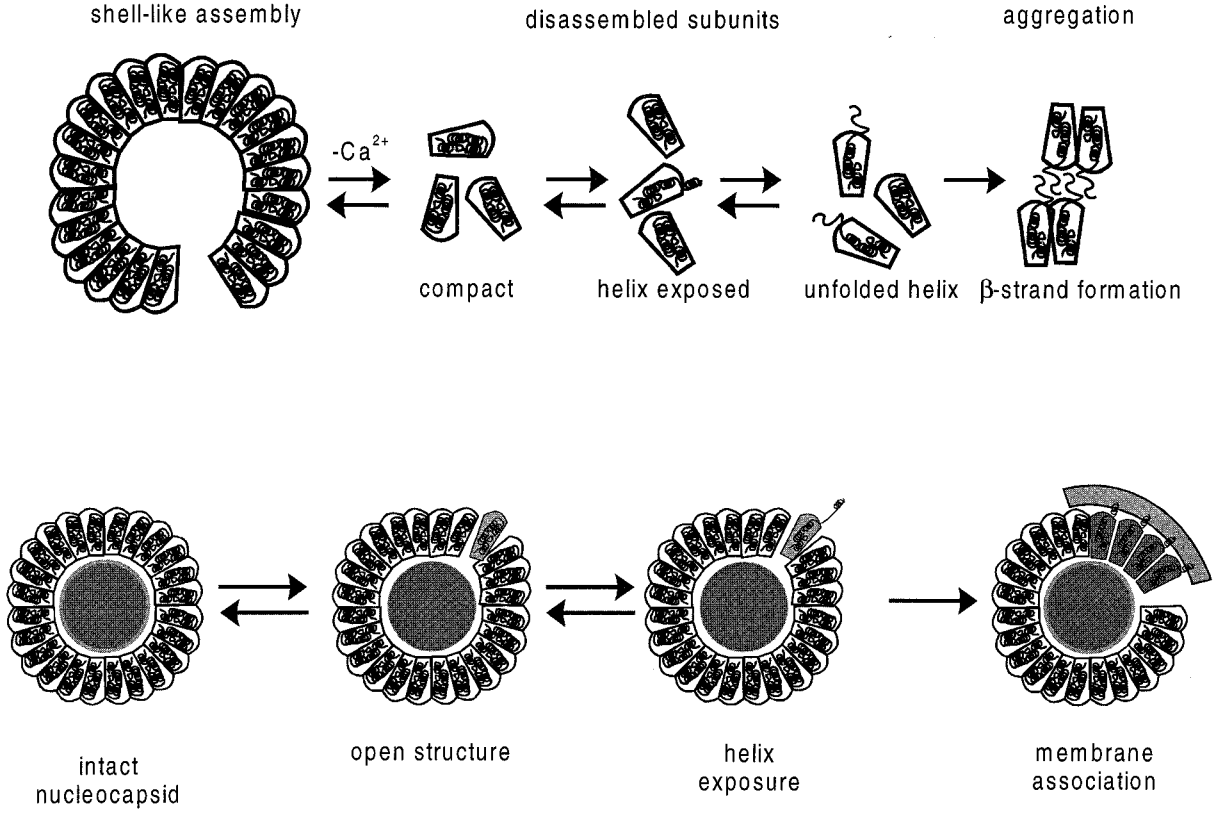

FIGURE 9: (Top) Proposed pathway for calcium-dependent disassembly of the P8 shell in vitro. Upon depletion of the Ca^{2+} concentration, a typical shell-like structure (left) disassembles rapidly into subunits, leading to exposure and local unfolding of a subunit α-helical domain. Subsequently, β-strand refolding and aggregation occur (right). (Bottom) Model of P8 subunit dynamics within the assembled shell and implications for cell entry and uncoating of the nucleocapsid. Subunit dynamics of the native shell (left) lead to a transiently open shell structure (grey-toned subunit) and an exposed helix domain that is capable of direct interaction with the membrane bilayer (right).

P8 Shell Assembly Is Mediated by Ca^{2+}. No change of secondary structure occurs in P8 immediately following NC shell disassembly and sequestration from Ca^{2+}. Thus, subunit−subunit interactions in the native NC shell lattice are likely stabilized by the binding of Ca^{2+}. Although the putative Ca^{2+}-binding sites of the P8 shell are not yet known, similar interactions have been demonstrated for other icosahedral viral lattices, including both plant viruses (*46*) and the bacteriophage ϕX174 (*47*). Acidic side chains Asp and Glu are considered the probable targets of Ca^{2+} binding.

Unlike plant viruses, in which divalent cations serve primarily to neutralize clusters of negatively charged residues, Ca^{2+} binding in the ϕ6 NC shell may fulfill a broader function. For example, Ca^{2+} is essential for stabilizing not only the P8 quaternary structure (NC shell) but also the subunit secondary structure. Surprisingly, despite global stabilization, the surface α-helices of the P8 subunit remain accessible to hydrogen-isotope exchange at native conditions. The surface lattice of the P8 shell thus largely retains the structural dynamics of the disassembled subunits, with local stability increasing by less than 2 kcal/mol. A similarity in dynamics has also been observed for the assembled shell and dissociated subunit (P3) states of the major coat protein of the dsDNA bacteriophage PRD1 (*48*). Both P3 of PRD1 and P8 of ϕ6 also exhibit in their disassembled states a substantial exchange-protected core (50−55% of all peptides). In contrast, the icosahedral capsid subunit (gp5) of bacteriophage P22 manifests significant increases in hydrogen-exchange protection upon initial assembly (procapsid shell) and maturation (capsid shell) (*16*). In contrast to P3 and P8, gp5 also exhibits diminished exchange protection in the disassembled subunit state (R. Tuma, P. E. Prevelige, and G. J. Thomas, Jr., unpublished results).

Assembly of the P8 Icosahedral Shell Requires a Polymerase Core Template. Because hydrogen-exchange protection of surface helices is not enhanced with P8 shell assembly, it can be concluded that local intersubunit interactions are intrinsically weak. Presumably, they do not constitute the primary driving force for the polymerization reaction. Whereas Ca^{2+} binding evidently augments the local intersubunit interactions that are necessary for assembly, shells formed in the absence of the core do not achieve closure (*6*). Thus, the polymerase core probably serves as the template that ensures correct form determination during P8 shell assembly. A similar mode of assembly was recently proposed for the closely related BTV core particle (*45*). The present work further suggests that the observed dynamic nature of intersubunit interactions in ϕ6 may be required for fidelity of alignment of subunits on the surface of the core template.

Subunit Aggregation Is Mediated by an α-Helix → β-Strand Transformation. Time-resolved Raman spectroscopy of the shell disassembly reaction indicates aggregation of P8 subunits mediated by a metastable α-helical secondary structure. The destabilized α-helices are slowly converted to β-strands during aggregation of disassembled subunits, in accordance with a mechanism like that depicted in the top panel of Figure 9. The P8 α-helices may also be temporarily exposed within the context of the assembled shell, as depicted in the bottom part of Figure 9, but the

subsequent aggregation is either sterically hindered or requires further unfolding of part of the folding core, which is stabilized by Ca^{2+} binding and assembly. This structure transformation of P8 subunits may be similar to the conversion of α-helical domains of amyloid-forming proteins into the extended network of β-strand structure that characterizes the amyloid state.

P8 Dynamics and Host Cell Entry. Intersubunit interactions of P8 within the NC shell are highly dynamic, in the sense that they do not protect specific structural domains against hydrogen exchange. This suggests transient opening and closing of channels between subunits of the shell lattice on a time scale that is long with respect to proton diffusion. A plausible biological role for this property is to facilitate membrane recognition and disassembly, as depicted in the lower panel of Figure 9. Here, we envisage the intact NC to comprise a structurally "compact" subunit state in equilibrium with a transiently "open" state, thus facilitating hydrogen exchange. The dynamic nature of such a subunit could provide the recognition sites required for membrane association during host cell entry. Temporal exposure of a buried α-helix has been observed for the flock house virus and was proposed to play a role in virion disassembly (*52*). A similar mechanism has also been proposed for poliovirus cell entry (*53*). The putative P8−membrane contacts would serve to destabilize the P8 lattice and lead ultimately to shell disassembly and release of the polymerase core.

ACKNOWLEDGMENT

We thank Ms. Marja-Leena Perälä for excellent technical assistance.

REFERENCES

1. Semancik, J. S., Vidaver, A. K., and Van Etten, J. L. (1973) *J. Mol. Biol. 78*, 617−625.
2. Vidaver, A. K., Koski, R. K., and Van Etten, J. L. (1973) *J. Virol. 11*, 799−805.
3. Romantschuk, M., Olkkonen, V. M., and Bamford, D. H. (1988) *EMBO J. 7*, 1821−1829.
4. Kakitani, H., Iba, H., and Okada, Y. (1980) *Virology 101*, 475−483.
5. Ktistakis, N. T., Kao, C.-Y., and Lang, D. (1988) *Virology*, 91−102.
6. Olkkonen, V. M., Ojala, P. M., and Bamford, D. H. (1991) *J. Mol. Biol. 218*, 569−581.
7. Emori, Y., Iba, H., and Okada, Y. (1980) *Mol. Gen. Genet. 180*, 385−389.
8. Mindich, L., and Davidoff-Abelson, R. (1980) *Virology 103*, 386-391.
9. Butcher, S. J., Dokland, T., Ojala, P. M., Bamford, D. H., and Fuller, S. D. (1997) *EMBO J. 16*, 4477−4487.
10. Bamford, J. K. H., Bamford, D. H., Li, T., and Thomas, G. J., Jr. (1993) *J. Mol. Biol. 230*, 473−482.
11. Ojala, P. M., Romantschuk, M., and Bamford, D. H. (1990) *Virology 178*, 364−372.
12. Li, T., Bamford, D. H., Bamford, J. K. H., and Thomas, G. J., Jr. (1993) *J. Mol. Biol. 230*, 461−472.
13. Overman, S., and Thomas, G. J., Jr. (1995) *Biochemistry 34*, 5440−5451.
14. Thomas, G. J., Jr. (1999) *Annu. Rev. Biophys. Biomol. Struct. 28*, 1−27.
15. Tuma, R., and Thomas, G. J., Jr. (1997) *Biophys. Chem. 68*, 17−31.
16. Tuma, R., Prevelige, P. E., Jr., and Thomas, G. J., Jr. (1998) *Proc. Natl. Acad. Sci. U.S.A. 95*, 9885−9890.
17. Tuma, R., Prevelige, P. E., Jr., and Thomas, G. J., Jr. (1996) *Biochemistry 35*, 4619−4627.
18. Prevelige, P. E., Jr., Thomas, D., Aubrey, K. L., Towse, S. A., and Thomas, G. J., Jr. (1993) *Biochemistry 32*, 537−543.
19. Juuti, J. T., Bamford, D. H., Tuma, R., and Thomas, G. J., Jr. (1998) *J. Mol. Biol. 279*, 347−359.
20. Bamford, D. H., Ojala, P. M., Frilander, M., Walin, L., and Bamford, J. K. H. (1995) *Methods Mol. Gen. 6*, 455−474.
21. Bradford, M. M. (1976) *Anal. Biochem. 72*, 248−254.
22. Olkkonen, V. M., and Bamford, D. H. (1989) *Virology 171*, 229−238.
23. Yang, J. T., Wu, C.-S. C., and Martinez, H. M. (1986) *Methods Enzymol. 130*, 208−269.
24. Tuma, R., and Thomas, G. J., Jr. (1996) *Biophys. J. 71*, 3454−3466.
25. Prevelige, P. E., Jr., Thomas, D., and King, J. (1993) *Biophys. J. 64*, 824−835.
26. Tuma, R., Parker, M. H., Weigele, P., Sampson, L., Sun, Y., Krishna, N. R., Casjens, S., Thomas, G. J., Jr., and Prevelige, P. E., Jr. (1998) *J. Mol. Biol. 281*, 81−94.
27. Bandekar, J. (1992) *Biochim. Biophys. Acta 1120*, 123−143.
28. Koenig, J. L., and Frushour, B. (1972) *Biopolymers 11*, 1871−1892.
29. Lord, R. C., and Yu, N. T. (1970) *J. Mol Biol. 51*, 203-213.
30. Miura, T., and Thomas, G. J., Jr. (1995) in *Subcellular Biochemistry. Proteins: Structure, Function and Engineering* (Biswas, B. B., and Roy, S., Eds.) pp 55−99, Plenum Press, New York.
31. Li, T., Chen, Z., Johnson, J. E., and Thomas, G. J., Jr. (1992) *Biochemistry 31*, 6673−6682.
32. Krimm, S., and Bandekar, J. (1986) *Adv. Protein Chem. 38*, 181−365.
33. Overman, S., and Thomas, G. J., Jr. (1998) *Biochemistry 37*, 5654−5665.
34. Overman, S., and Thomas, G. J., Jr. (1998) *J. Raman Spectrosc. 29*, 23−29.
35. Berjot, M., Marx, J., and Alix, A. J. P. (1987) *J. Raman Spectrosc. 18*, 289−300.
36. Thomas, G. J., Jr., and Agard, D. A. (1984) *Biophys. J. 46*, 763−768.
37. Siamwiza, M. N., Lord, R. C., Chen, M. C., Takamatsu, T., Harada, I., Matsuura, H., and Shimanouchi, T. (1975) *Biochemistry 14*, 4870−4876.
38. Lin-Vien, D., Colthup, N. B., Fateley, W. G., and Grasselli, J. G. (1991) *The Handbook of Infrared and Raman Characteristic Frequencies of Organic Molecules*, Academic Press, San Diego.
39. Fasman, G. D., Itoh, K., Liu, C. S., and Lord, R. C. (1978) *Biopolymers 17*, 1729−1746.
40. Wingfield, P. T., Stahl, S. J., Williams, R. W., and Steven, A. C. (1995) *Biochemistry 34*, 4919−4932.
41. Momany, C., Kovari, L. C., Prongay, A. J., Keller, W., Gitti, R. K., Lee, B. M., Gorbalenya, A. E., Tong, L., McClure, J., Ehrlich, L. S., Summers, M. F., Carter, C., and Rossmann, M. G. (1996) *Nat. Struct. Biol. 3*, 763−770.
42. Gamble, T. R., Yoo, S., Vajdos, F. F., von Schwedler, U. K., Worthylake, D. K., Wang, H., McCutcheon, J. P., Sundquist, W. I., and Hill, C. P. (1997) *Science 278*, 849−853.
43. Zlotnick, A., Stahl, S. J., Wingfield, P. T., Conway, J. F., Cheng, N., and Steven, A. C. (1998) *FEBS Lett. 431*, 301−304.
44. Grimes, J., Basak, A. K., Roy, P., and Stuart, D. (1995) *Nature 373*, 167−170.
45. Grimes, J. M., Burroughs, J. N., Gouet, P., Diprose, J. M., Malby, R., Zientara, S., Mertens, P. P., and Stuart, D. I. (1998) *Nature 395*, 470−478.
46. Gilbert, J. M., and Greenberg, H. B. (1997) *J. Virol. 71*, 4555−4563.
47. Speir, J. A., Munshi, S., Wang, G., Baker, T. S., and Johnson, J. E. (1995) *Structure 3*, 63−78.
48. McKenna, R., Xia, D., Willingmann, P., Ilag, L. L., and Rossmann, M. G. (1992) *Acta Crystallogr., Sect. B 48*, 499−511.

49. Tuma, R., Bamford, J. K. H., Bamford, D. H., Russell, M. P., and Thomas, G. J., Jr. (1996) *J. Mol. Biol. 257*, 87−101.
50. Sugawara, J., Harada, I., Matsuura, H., and T., S. (1978) *Biopolymers 17*, 1405−1421.
51. Yu, T.-J., Lippert, J. L., and Peticolas, W. L. (1973) *Biopolymers 12*, 2161−2176.
52. Bothner, B., Dong, X. F., Bibbs, L., Johnson, J. E., and Siuzdak, G. (1998) *J. Biol. Chem. 273*, 673−676.
53. Tosteson, M. T., and Chow, M. (1997) *J. Virol. 71*, 507−511.

BI991473P